ATLANTIS PRESS

Advances in Engineering Research, volume 110

3rd Annual International Conference on Advanced Material Engineering (AME 2017)

Effect of Single SiO_2 Layer Incorporation on Electrical Performances of Metal-insulator-metal Capacitors with Al_2O_3-HfO_2-Al_2O_3 Dielectrics

Li-Feng ZHANG[a] and Sai-Sheng XU[b]

State Key laboratory of ASIC and System, School of Microelectronics, Fudan University, Shanghai 200433, China

[a]lfzhang@fudan.edu.cn [b]ssxu@fudan.edu.cn

Keywords: MIM (metal-insulator-metal), VCC (voltage coefficients of capacitance), ALD (atomic layer deposition).

Abstract. The metal-insulator-metal (MIM) capacitors with $Al_2O_3/HfO_2/Al_2O_3$ (AHA) and $Al_2O_3/HfO_2/SiO_2/HfO_2/Al_2O_3$ (AHSHA) dielectric structure using atomic layer deposition (ALD) technique have been fabricated. It is demonstrated that the dielectric loss at higher applied frequency and quadratic VCC in high-κ MIM capacitors can be decreased by means of introducing an ultrathin layer of ALD SiO_2, which has an opposite sign of quadratic VCC against the HfO_2 layers. A high capacitance density of 8.1 fF/μm^2 and the low leakage current density of 2.5□ 10-7 A/cm^2 at 1 MV/cm can be achieved with the dielectric structure as AHSHA. In addition, the breakdown electrical field in AHSHA dielectric is obviously improved. Furthermore, with the survey of different leakage models, the Schottky emission has been considered as the dominating conduction mechanism for both of the AHA and AHSHA capacitors.

Introduction

High-permittivity (high-κ) metal-insulator-metal (MIM) capacitors have recently been studied for RF and analog/mixed-signal integrated circuits [1-7]. Among high-κ materials, HfO_2 is one of the most promising candidates due to high-κ (about 20-25) and large band gap (5.7 eV) [8-10]. However, a relatively high quadratic voltage coefficients of capacitance (α) remains as a serious dilemma for the application of the HfO_2 MIM capacitors, where the α is known to be inversely proportional to dielectric thickness and dielectric constant [11-13]. So that, the α and capacitance density have a trade-off relationship. Meanwhile, as for conventional dielectric materials of MIM capacitors, SiO_2 and Si_3N_4 are commonly used materials although it is hard to achieve high capacitance density due to their low dielectric constant κ (about 4-7) [4, 14, 15]. Therefore, in order to obtain high capacitance density, relatively low α and low leakage current density, it seems to be a good choice to incorporate single SiO_2 or Si_3N_4 layer into high-κ sandwiched dielectric materials of MIM capacitors.

In addition, due to the requirement of the MIM capacitors embedded into the inter-level dielectric layers, the maximum fabrication temperature of the MIM capacitors should be compatible with the thermal budget (<450 ^{0}C) of Cu back-end-of-line process. Of the various high-κ dielectric deposition techniques, atomic layer deposition (ALD) technique, which has some outstanding advantages such as exquisite control over the film composition and structure, high uniformity and perfect conformity, can satisfy the low temperature requirement. So far, many reports have been focused on high—κ deposition with ALD, where well properties of high capacitance density, small voltage coefficient of capacitance and low leakage current were observed [16, 17]. However, there has been little study on the effect of single SiO_2 in high-κ sandwiched dielectrics deposited by ALD in advanced MIM capacitors.

In this paper, we show that the α of $Al_2O_3/HfO_2/Al_2O_3$ dielectric MIM capacitance can be decreased by introducing an ultrathin SiO_2 layer deposited by ALD, which has an opposite sign of the α. The ALD Al_2O_3 layer is deposited as the contact layer between dielectric and electrodes in order to obtain the low leakage current density of the MIM capacitors. Meanwhile, different current leakage models have been used to fit the experimental data in order to investigate the dominating conduction mechanism.

Experimental

A 150 nm TiN was grown on the 500 nm thermal oxide/Si substrate by sputtering, served as the bottom electrode. Subsequently, the TiN coated wafers were transferred into the ALD chamber for the dielectric growth. Al_2O_3 and HfO_2 were grown with thermal ALD process from Al $(CH_3)_3$/H2O and $Hf(N(CH_3)(C_2H_5))_4/H_2O$, respectively. The single SiO_2 layer was deposited by plasma enhanced ALD process from the precursor of Trisdimethylamino-silane (TDMAS: $SiH(N(CH_3)_2)_3$) and O_2, with the plasma power of 100 W. During the process, the reactor chamber temperature was set at 200^{o}C, and all of the vapors of precursors were delivered into the reactor chamber with N_2 gas as carrier. The dielectric thickness was measured by an ellipsometer. Finally, the top electrode with 100 μm diameter of sputtered Ta was formed with lift-off method. The MIM capacitors with two structures of dielectric layers [A (1nm)/H(11nm)/A(1nm), A(1nm)/H(5nm)/S(1nm)/H(5nm)/A(1nm), A, H and S denoted as Al_2O_3, HfO_2, and SiO_2, respectively] were fabricated to investigate the effect of the intermediate SiO_2 layer. And then we denoted them as AHA and AHSHA capacitors, respectively. Capacitance-voltage (C-V) measurements were carried out with LCR meter (Keilthley 4200) with 100-mV ac sweeping signal. The leakage current characteristics were measured by using semiconductor device analyzer (Agilent B1500A).

Results and Discussion

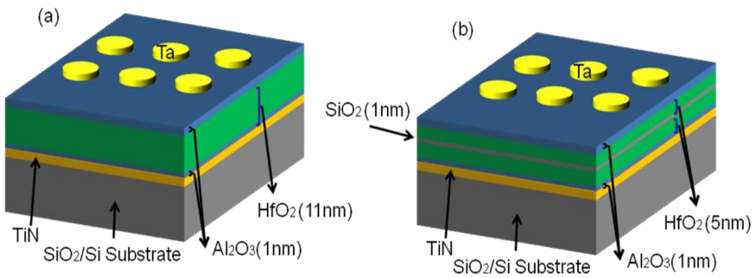

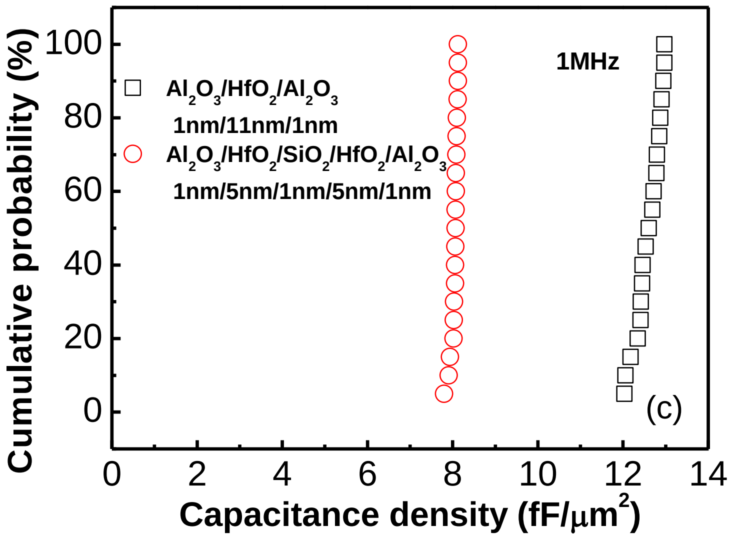

Fig. 1 (a) Schematic diagram of the AHA MIM capacitor; (b) Schematic diagram of the AHSHA MIM capacitor; (c) Cumulative distributions of capacitance densities of both MIM capacitors

Fig. 1 shows the schematic diagrams of AHA and AHSHA MIM capacitors and the cumulative distributions of the measured capacitance densities at 0 V under 1 MHz for both capacitors. The resulting capacitance density equals 12.6 and 8.1 fF/μm2 for the AHA and AHSHA capacitors at 50% cumulative probability, respectively. It can be found that with the introduction of the SiO_2 layer, the capacitance density decreases as expected. The dielectric constants can be calculated as 18.4 and 11.9 according to the capacitance density for the AHA and AHSHA capacitors, separately. For the AHA capacitor, the dielectric constant is in accordance with other reports [4, 11, 18]; while with the introduction of single SiO_2 layer, the dielectric constant drops. The frequency dependences of capacitance densities for both capacitors at 0 V dc bias is shown in Fig. 2, together with the dissipation factor. It can be observed that the capacitance densities are relatively stable as the measurement frequency varied from 1 KHz to 1 MHz, indicating their excellent dielectric characteristics with frequency. Meanwhile, the variation of the dissipation factor along with frequency (as shown in Fig. 2) implies AHSHA structure capacitor with 1 nm intermediate SiO_2 layer can effectively reduce dielectric loss relative to AHA structure capacitor at higher applied frequency.

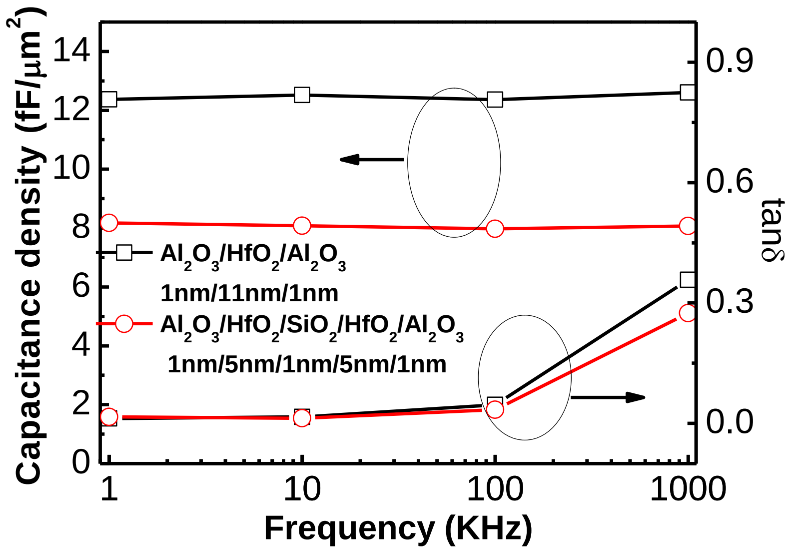

Fig. 2 The capacitance densities as a function of frequency for both capacitors, together with the dissipation factor.

The voltage coefficients of capacitance (VCC) are very important parameters for the application of MIM capacitors to radio frequency circuits, which can be determined by using Eq. (1) to fit the experimental data:

$$C(V) = C_0(\alpha V^2 + \beta V + 1), \tag{1}$$

Where C_0 is the measured capacitance at 0 V, α and β represent quadratic and linear VCC, respectively.

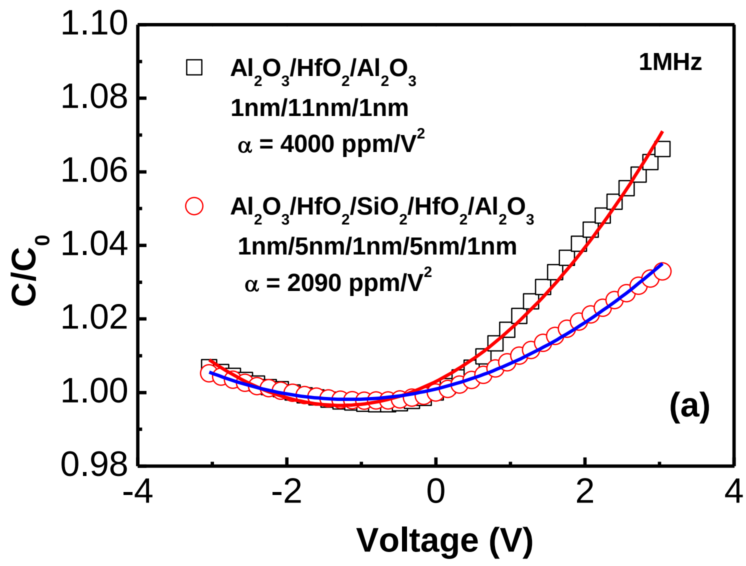

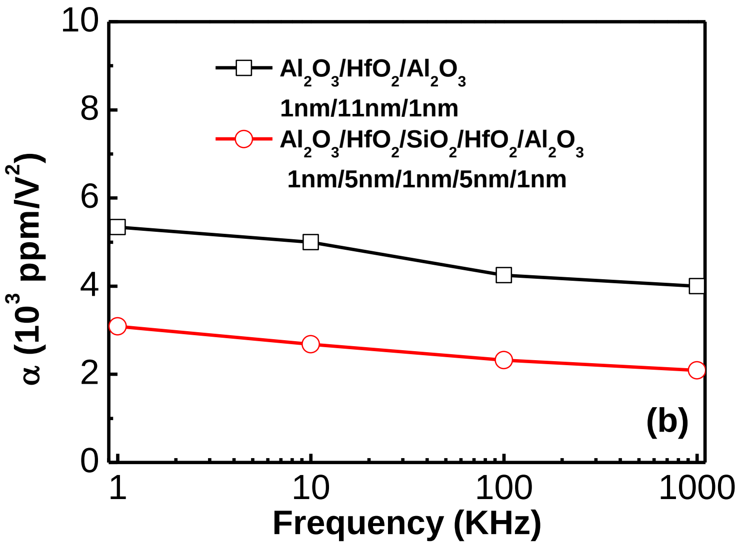

Fig. 3 (a). Typical plotting of C/C_0 versus voltage at 1 MHz for both capacitors, together with the fitted curves; (b). Quadratic Vcc as a function of frequency for both capacitors.

The typical normalized capacitances (C/C_0) versus dc bias measured at 1 MHz for both capacitors together with the fitted curves have been shown in Fig. 3(a). It is found that the α value is 4000 ppm/V^2 for the AHA capacitor; while the α is decreased to 2090 ppm/V^2 evidently with the introduction of the 1nm SiO_2 layer in AHSHA capacitor, as it is predicted. The asymmetric of the curves for dc bias maybe result from the oxidation of the bottom TiN electrode, which leads to the relatively large VCC due to electron injection from bottom electrode under positive bias voltage [16-18]. At the same time, a better VCC characteristic in AHSHA capacitor can be obviously found, but a worse one in AHA capacitor under positive bias voltage. Fig. 3(b) exhibits the α as a function of frequency for both capacitors. For the AHA capacitor, the α value varies from 5340 to 4000 ppm/V2 with the measurement frequency increasing from 1 KHz to 1 MHz. And for the AHSHA capacitor, the α value varies from 3090 to 2090 ppm/V2 with the measurement frequency increasing from 1 KHz to 1 MHz. This results clearly demonstrate the α value is strongly affected by the frequency and decreasing with frequency increase, in agreement with other reports [4, 16].

The typical leakage current density (J) of the capacitors as a function of electric field (E) measured at room temperature is shown in Fig. 4. It is observed that the AHSHA capacitor exists the much higher breakdown field than that of the AHA capacitor. This indicates that the intermediate SiO_2 layer is very effective for improving the dielectric breakdown strength, because SiO_2 has an amorphous state and a large band gap (9 eV) in a universal IC process temperature range [14]. Ding et al. have reported that the crystallization of HfO_2 can be enhanced with increasing its thickness [8]. So with the introduction of the intermediate SiO_2 layer, the crystallization of HfO_2 can be suppressed and the grain boundaries (highly leaky paths) can be decreased, in order to lead to high electrical breakdown strength [19]. Meanwhile, the decrease of leakage current density is found with the introduction of SiO_2 layer, where the leakage current density is 8.1×10^{-7} A/cm^2 at 1 MV/cm for the AHA capacitor and the leakage current density of the capacitor decreases to 2.5×10^{-7} A/cm^2 at 1MV/cm with the introduction of the 1 nm intermediate SiO_2 in AHSHA capacitor, when it maintains the fixed physics thickness of the insulator. Furthermore, the small asymmetry of the leakage current density has been found as a function of the electric field for both capacitors, which may be caused by the different work function of the electrodes.

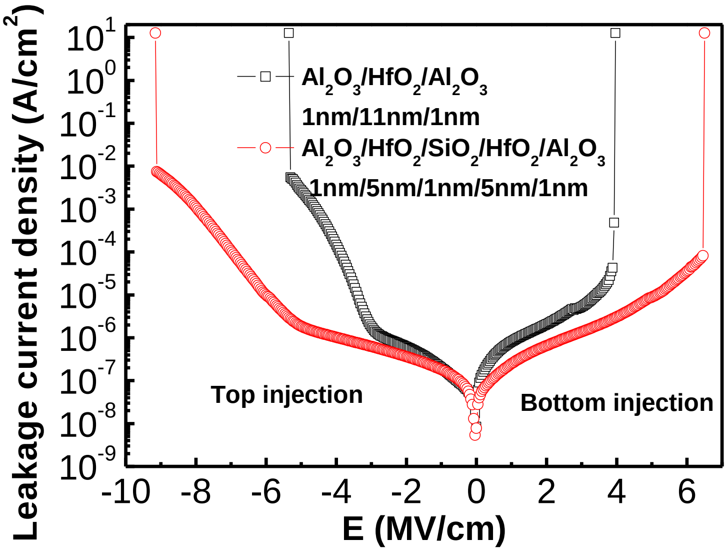

Fig. 4 Dependence of leakage current density on electric field for both capacitors.

In order to investigate the intrinsic physics of the leakage current, we survey the general leakage mechanisms at present including Schottky emission and Poole-Frenkel (PF) emission [4, 14]. According to Schottky emission arising from a difference in Fermi level between a metal and a semiconductor, charges have to overcome the potential barrier created by the energy difference between the metal and semiconductor [4, 20, 21]. The current density (Js) can be expressed as

$$J_s = AT^2 \exp\left(-\frac{\varphi - \sqrt{q^3 E / 4\pi\varepsilon_0\varepsilon_r}}{k_B T}\right), \tag{2}$$

where A is the Richardson constant, T is the temperature, φ is the height of the Schottky barrier, q is the electronic charge, ε_0 is the permittivity of free space, ε_r is the dynamic relative dielectric constant, and k_B is the Boltzmann constant. For Poole-Frenkel (PF) emission, it involves the thermal ionization of trapped carriers into the conduction of thin films [14, 21], and can be expressed as

$$J_{PF} = BE \exp\left(-\frac{E_I - \sqrt{q^3 E / \pi\varepsilon_0\varepsilon_r}}{k_B T}\right), \tag{3}$$

Where B is the constant, E_I is the trap ionization energy. Fig. 5 exhibits the typical plotting of *ln (J) vs* $E^{1/2}$ for the AHA and AHSHA capacitors under electron bottom injection according to the Schottky emission. It is observed that the experimental data can be well linearly fitting with

Schottky emission model and the relative dielectric constants (ε_r) for AHA and AHSHA dielectrics are deduced around 26.8 and 24.5, which are slightly larger than the previous calculated dielectric constant 18.4 and 11.9 by C-V measurement; while both of the deduced relative dielectric constants for AHA and AHSHA are over 30 with PF emission model (not shown here), which are far larger than values of theory and C-V measurement [8-10]. This result demonstrates the Schottky emission dominates the conduction for both of AHA and AHSHA capacitors, in agreement with the observation in AHA capacitor by Ding et al [4].

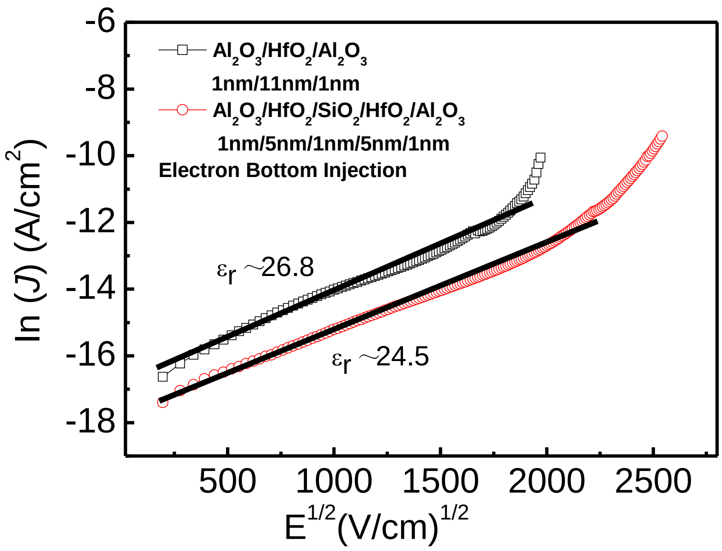

Fig. 5 Typical plotting of ln(J) vs E1/2 for the AHA and AHSHA capacitors according to the Schottky emission, and the deduced relative dielectric constants (ε_r).

Conclusions

The $Al_2O_3/HfO_2/Al_2O_3$ dielectric MIM capacitors with the SiO_2 intermediate layer have been fabricated with ALD technology. The decrease of the quadratic voltage coefficient of HfO_2 MIM capacitance by introducing an ultrathin SiO_2 layer has been realized in our experiment. Meanwhile, it is found that the properties of the dielectric loss and leakage density can be obviously improved. Moreover, the Schottky emission is responsible for the dominating conduction mechanism for both of AHA and AHSHA MIM capacitors.

Acknowledgments

This work was supported by the National Natural Science Foundation of China (61076076), and the China Postdoctoral Science Foundation (No. 2014M551323).

References

[1] Sang. Uk. Park, Chang. Yong. Kang, Hyuk. Min. Kwon, Byung. Seok. Park, Won. Ho. Choi, In. Shik. Han, Gennadi. Bersuker, Raj. Jammy, Hi. Deok. Lee. Analysis of reliability characteristics of high capacitance density MIM capacitors with SiO2–HfO2–SiO2 dielectrics. Microelectronic Engineering 2011; 88: 3389-3392.

[2] J. Robertson. Maximizing performance for higher K gate dielectrics. J. Appl. Phys 2008; 104: 124111-6.

[3] K. Tomida, K. Kita, A. Toriumi. Dielectric constant enhancement due to Si incorporation into HfO2. Appl. Phys. Lett 2006; 89: 142902-3.

[4] S. J. Ding, C. X. Zhu, M. F. Li, D. W. Zhang. Atomic-layer-deposited Al2O3-HfO2-Al2O3 dielectrics for metal-insulator-metal capacitor applications. Appl. Phys. Lett 2005; 87: 053501-3.

[5] Y. L. Tu, L. Lin, L. L. Chao, D. Wu, C. S. Tsai, C. Wang, C. F. Huang, C. H. Lin, J. Sun. Symp. Characterization and comparison of high-k metal-insulator-metal (MIM) capacitors in 0.13 um Cu BEOL for mixed-mode and RF applications. VLSI Tech Dig 2003; p. 79-80.

[6] H. Hu, S. J. Ding, H. F. Lim, C. Zhu, M. F. Li, S. J. Kim, X. F. Yu, J. H. Chen, Y. F. Yong, B. J. Cho, D. S. H. Chan, S. C. Rustagi, M. B. Yu, C. H. Tung, A. Du, D. My, P. D. Foo, A. Chin, D. L. Kwong. High performance ALD HfO2-Al2O3 laminate MIM capacitor for RF and mixed signal IC application. IEDM Tech. Dig 2003; p. 379-382.

[7] T. Ishikawa, D. Kodama, Y. Matsui, M. Hiratani, T. Furusawa, D. Hisamoto. High-capacitance Cu/Ta2O5/Cu MIM structure for SoC application featuring a single-mask add-on process. IEDM Tech. Dig 2002; p. 940-942.

[8] S. J. Ding, J. Xu, Y. Huang, Q. Q. Sun, D. W. Zhang, M. F. Li. Electrical characteristics and conduction mechanisms of metal-insulator-metal capacitors with nanolaminated Al2O3-HfO2 dielectrics. Appl. Phys. Lett 2008; 93: 092909-3.

[9] M. Balog and M. Schieber. Chemical vapor deposition and characterization of HfO2 films from organo-hafnium compounds. Thin. Solid. Films 1977; 41: 247-259.

[10] G. D. Wilk, R. M. Wallace, and J. M. Anthony. High-κgate dielectrics: Current status and materials properties considerations. J. Appl. Phys 2001; 89: 5243-5275.

[11] Ho.Young. Kwak, Hyuk. Min. Kwon, Yi. Jung. Jung, Sung. Kyu. Kwon, Jae. Hyung. Jang, Woon. Il. Choi, Man. Lyun. Ha, Ju. Il. Lee, Song. Jae. Lee, Hi. Deok. Lee. Characterization of Al2O3–HfO2–Al2O3 sandwiched MIM capacitor under DC and AC stresses. Solid. State. Electronics 2013; 79: 218-222.

[12] D. Kannadassan, R. Karthik, Maryam. Shojaei. Baghini, P. S. Mallick. Modeling the voltage nonlinearity of high-k MIM capacitors. Solid. State. Electronics 2014; 91: 112-117.

[13] Wenger. C, Lupina. G, Lukosius M, Seifarth. O, Mussig H, Pasko. S, et al. Microscopic model for the nonlinear behavior of high-k metal–insulator–metal capacitors. J. Appl. Phys 2008; 103 (10).

[14] Qiu. Xiang. Zhang, Bao. Zhu, Li. Feng. Zhang, Shi. Jin. Ding. Atomic-layer-deposited SiO2/TiO2/SiO2 sandwiched dielectrics for metal–insulator–metal capacitor application. Microelectronic Engineering 2014; 122: 1-4.

[15] Sun. Jung. Kim, Byung. Jin. Cho, Ming. Fu. Li, Shi. Jin. Ding, Chunxiang. Zhu, Ming. Bin. Yu, Babu. Narayanan, Albert. Chin, and Dim. Lee. Kwong. Improvement of Voltage Linearity in High-k MIM Capacitors Using HfO2–SiO2 Stacked Dielectric. Electron Device Letters 2004; 25: 538-540.

[16] H. Hu, C. Zhu, Y. F. Lu, M. F. Li, B. J. Cho, and W. K. Choi. A High Performance MIM Capacitor Using HfO2 Dielectrics. IEEE Electron Device Lett 2002; 23: 514-516.

[17] T. K. Kang, C. W. Chen, C. L. Lin, W. F. Wu. Effect of Thermal Annealing or Plasma Treatment on Analog Characteristics for High-k Material Capacitors. Jpn. J. Appl. Phys 2008; 47: 5374-5379.

[18] Tsung. Kuei. Kang, Chia. Tung. Chang, Cheng. Li. Lin, Wen. Fa. Wub. Influences of bottom electrode TaN on electrical characteristics for metal–HfO2–metal capacitors. Microelectronic Engineering 2009; 86: 1994-1998.

[19] G. Bersuker, J. Yuma, L. Vandelli, A. Padovani, L. Larcher, V. Iglesias, M. Porti, M. Nafría, K. McKenna, A. Shluger, P. Kirsch, R. Jammy. Grain boundary-driven leakage path formation in HfO2 dielectrics. Solid. State. Electronics 2011; 65-66: 146-150.

[20] J.Wu, and J.Wang. Diodelike and resistive hysteresis behavior of heterolayered BiFeO3/ ZnO ferroelectric thin films. J. Appl. Phys 2010; 108: 094107-7.

[21] Z. H. Chen, L. He, F. Zhang, J. Jiang, J. W. Meng, et al. The conduction mechanism of large on/off ferroelectric diode currents in epitaxial (111) BiFeO3 thin film. J. Appl. Phys 2013; 113: 184106.